IEEE Press Series on Power and Energy Systems
Ganesh Kumar Venayagamoorthy, Series Editor

Practical Partial Discharge Measurement on Electrical Equipment

Greg C. Stone, Andrea Cavallini, Glenn Behrmann,
Claudio Angelo Serafino

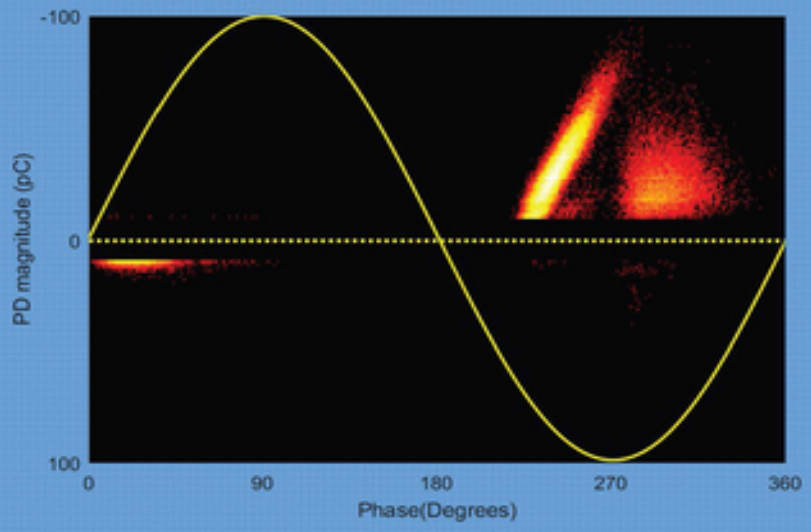

IEEE PRESS

WILEY

Table of Contents

- Cover
- Table of Contents
- Series Page
- Title Page
- Copyright Page
- Dedication Page
- About the Authors
- Preface
- Acknowledgments
- Acronyms
- 1 Introduction
  - 1.1 Why Perform Partial Discharge Measurements?
  - 1.2 Partial Discharge and Corona
  - 1.3 Categories of PD Tests
  - 1.4 PD Test Standards
  - 1.5 History of PD Measurement
  - 1.6 The Future
  - 1.7 Roadmap for the Book
  - References*
- 2 Electric Fields and Electrical Breakdown
  - 2.1 Electric Fields in High-Voltage Equipment
  - 2.2 Electrical Breakdown
  - 2.3 Breakdown in Gases
  - 2.4 Breakdown in Solids
  - 2.5 Breakdown in Liquids

2.6 Dielectric Strength
References
3 Physics of Partial Discharge
3.1 Introduction
3.2 Classification of Partial Discharges
3.3 PD Current Pulse Characteristics
3.4 Effects of PD
3.5 Corona Due to Non-Uniform Electric Fields Around Conductors
3.6 Partial Discharge in Voids
3.7 PD on Insulation Surfaces
3.8 Effect of Ambient Conditions and Conditioning
3.9 Summary of Measured PD Quantities
3.10 Understanding the PD Pattern with Respect to the AC Cycle
References
4 Other Discharge Phenomena
4.1 Introduction
4.2 PD as Interference
4.3 Circuit Breaker Arcing
4.4 Contact Arcing and Intermittent Connections
4.5 Metal Oxide Layer Breakdown
4.6 Dry Band Arcing
4.7 Glow (or Pulseless) Discharge
References
5 PD Measurement Overview
5.1 Introduction
5.2 Charge-Based and Electromagnetic Measurement Methods

5.3 Optical PD Detection
5.4 Acoustic Detection of PD
5.5 Chemical Detection
References
6 Charge-Based PD Detection
6.1 Introduction
6.2 Basic Electrical Detection Circuits Using Coupling Capacitors
6.3 Measuring Impedances
6.4 Electrical PD Detection Models
6.5 Quasi-integration in Charge-Based Measuring Systems
6.6 Calibration into Apparent Charge
References
7 Electromagnetic (RF) PD Detection
7.1 Why Measure Electromagnetic Signals from PD
7.2 Terminology
7.3 Basic Electrical Detection Circuits
7.4 Types of RF Sensors
7.5 Measuring Instruments
7.6 Performance and Sensitivity Check
7.7 PD Source Location
References
8 PD Measurement System Instrumentation and Software
8.1 Introduction
8.2 Frequency Range Selection
8.3 PD Detector Hardware Configurations

8.4 Hardware-Based Interference Suppression and PD Source Identification
8.5 PD Calibrator Hardware
8.6 Special Hardware Requirements for Continuous Monitors
8.7 PD System Output Charts
8.8 PD Activity Indicators
8.9 Post-Processing Software for Interference Suppression and PD Analysis
References
9 Suppression of External Electrical Interference
9.1 Impact of External Electrical Interference
9.2 Typical Sources of Noise and External Electrical Interference
9.3 Interference Suppression for Offline PD Testing
9.4 Online Interference Suppression
References
10 Performing PD Tests and Basic Interpretation
10.1 Introduction
10.2 PDIV/PDEV Measurement
10.3 PD Magnitude and PRPD Test Procedure
10.4 Interpretation of PD Magnitude
10.5 PRPD Pattern Interpretation
10.6 PD Root Cause Identification Using Changes in Ambient and Operating Conditions
References
11 PD Testing of Lumped Capacitive Test Objects
11.1 Lumped Capacitive Objects
11.2 Test Procedures

11.3 Measures to Suppress Electrical Interference
11.4 Sensitivity Check
References
12 PD in Power Cables
12.1 Introduction
12.2 Cable System Structure
12.3 Cable System Failure Mechanisms
12.4 Cable PD Test Standards
12.5 PD Test Sensors
12.6 PD Pulse Propagation and Detector Bandwidth
12.7 Factory Quality Assurance (QA) Testing of Power Cable
12.8 Energizing Cables in Offline/Onsite PD Tests
12.9 Offline/Onsite Testing
12.10 Pros and Cons of Offline Versus Online PD Measurements for Condition Assessment
12.11 Online Monitoring
12.12 Interference Separation
12.13 PRPD Patterns
12.14 PD Source Localization
References
13 Gas-Insulated Switchgear (GIS)
13.1 Introduction
13.2 Relevant Standards and Technical Guidance
13.3 The GIS Insulation System
13.4 Typical PD Sources in GIS and their Failure Modes
13.5 Detection of PD in GIS
13.6 Charge-Based PD Measurement in GIS

13.7 Application of Acoustic Techniques for PD Measurement on GIS
13.8 Radio-Frequency PD Measurement on GIS: The UHF Method
13.9 GIS Routine Factory Test
13.10 Onsite PD Measurement of GIS
13.11 Online Continuous PD Monitoring (PDM) of GIS
13.12 GIS PD Signal Examples and PRPD Patterns
13.13 HVDC GIS: Special Considerations
References
14 Air-Insulated Switchgear and Isolated Phase Bus
14.1 Introduction
14.2 AIS Insulation Systems
14.3 Insulation Failure Processes
14.4 PD Sensors
14.5 Commissioning and Offline/Onsite Testing
14.6 Online PD Monitoring
14.7 PD Interpretation for AIS
14.8 PD Measurement in Isolated Phase Bus
References
15 Power Transformers
15.1 Introduction
15.2 Transformer Insulation Systems
15.3 Typical Causes of PD in Dry-Type (Cast Resin) Transformers
15.4 Typical Causes of PD in Oil-Filled Transformers
15.5 Relevant Standards

15.6 PD Pulse Propagation and PD Detection in Transformers
15.7 Sensors for PD Detection
15.8 AC Supply for Offline Testing
15.9 Precautions Against Background Noise and Interference in Electrical PD Testing
15.10 Factory Acceptance Testing of Transformers
15.11 Onsite Offline Testing
15.12 Online PD Monitoring
15.13 Typical PRPD Patterns
References
16 Rotating Machine Stator Windings
16.1 Introduction
16.2 Relevant Standards
16.3 Stator Winding Insulation Systems
16.4 Stator Winding Insulation Failure Processes
16.5 PD Pulse Propagation in Stator Windings
16.6 PD Sensors
16.7 Factory Acceptance Testing
16.8 Onsite Offline Tests
16.9 Online Testing and Monitoring
16.10 Differences Between Online and Offline Tests
16.11 Interpretation
16.12 Root Cause Identification
16.13 Locating PD Sites
References
17 PD Detection in DC Equipment
17.1 Why Is HVDC So Popular Now?
17.2 Insulation System Design in DC

17.3 The Reasons for PD Testing Using DC
17.4 Offline PD Testing with DC Excitation
17.5 Interpretation of PD Measurements Under DC Excitation
17.6 Perspective
References
18 PD Detection Under Impulse Voltage
18.1 Introduction
18.2 Insulation Failure Due to Short Risetime Impulse Voltages
18.3 Electrical PD Detection
18.4 Nonelectrical Sensors
18.5 PD Display and Quantities Measured
18.6 Sensitivity and Interference Check
18.7 Test Procedures
18.8 Interpretation
References
Index

IEEE Press Series on Power and Energy Systems
End User License Agreement

List of Tables

Chapter 2
Table 2.1 Laws governing electrostatic fields.
Table 2.2 Relative permittivity of some industrial dielectrics.

Table 2.3 Peak dielectric strength of some dielectrics.

Chapter 3

Table 3.1 Main differences between Townsend and streamer discharges [3].

Chapter 6

Table 6.1 Frequency range for quasi-integration.

Chapter 7

Table 7.1 Classification of radiated EM signals.

Table 7.2 Different components of a VHF/UHF detection systems.

Table 7.3 Performance and sensitivity checks of VHF/UHF detection systems....

Chapter 8

Table 8.1 Q_{IEC} response of IEC 60270 systems to a series of pulses.

Chapter 12

Table 12.1 Summary of standards for cable testing and their aim.

Table 12.2 Test conditions and pass/fail criteria for cables with an age <5...

Table 12.3 Test conditions and pass/fail criteria for aged cables.

Chapter 13

Table 13.1 Acoustic properties of some of the materials used in GIS.

Chapter 15

Table 15.1 Main properties of different transformer insulating liquids.

Table 15.2 Main properties of insulating papers.

Table 15.3 Main properties of transformer board.

Table 15.4 Example of the cross-coupling between phases and between HV and ...

Chapter 16

Table 16.1 Statistical distributions found in air-cooled machines as a func...

Table 16.2 Characteristics of the PRPD features and the effect of operating...

List of Illustrations

Chapter 1

Figure 1.1 Plot of the number of papers on PD and corona vs year of publicat...

Figure 1.2 Recent photograph of a still-working ERA Model 3S, manufactured b...

Figure 1.3 Oscilloscope photograph of a single PD current pulse through a 50...

Figure 1.4 Photograph of the first commercial digital PD instrument that mea...

Chapter 2

Figure 2.1 Example of equipotential lines in an electrode configuration (whi...

Figure 2.2 High-voltage test circuit: 1.4 MV HVDC generator in Terrasa, Spai...

Figure 2.3 Coaxial cylindrical electrodes.

Figure 2.4 Electric field at the point electrode.

Figure 2.5 Schematic representation of the three major types of cavities: (a...

Figure 2.6 Schematic representation of an interface.

Figure 2.7 Tracking in a XLPE cable joint.

Figure 2.8 Electric field at a triple point of (for example) epoxy, air, and...

Figure 2.9 Bad, (a) and (b), versus good, (c) and (d) electrode configuratio...

Figure 2.10 Schematic representation of a Townsend avalanche.

Figure 2.11 Townsend effective ionization coefficient as a function of elect...

Figure 2.12 Paschen curve. Expression #1 is derived using Equation (2.22), w...

Figure 2.13 Electric field in proximity of a Townsend avalanche ($E_0 = V/d$)....

Figure 2.14 Corona discharge on corona ring of 500 kV overhead power line, p...

Figure 2.15 Examples of V-t characteristics for cylindrical coaxial electrod...

Figure 2.16 V-t characteristic of solid insulation.

Figure 2.17 Various shapes of electrical trees grown from a needle, reconstr...

Figure 2.18 Example of an electrical treeing in a polyethylene power cable....

Figure 2.19 Treeing starting from a millimeter size cavity in epoxy resin.

Figure 2.20 Formation of cellulose fiber bridges in mineral oil under mildly...

Figure 2.21 V-t characteristic of liquids. *Source:* Mahmud et al. (2014) / IE...

Figure 2.22 Breakdown strength of air as a function of gap length (derived f...

Chapter 3

Figure 3.1 Classification of partial discharge phenomena.

Figure 3.2 Alternative classification of partial discharge phenomena.

Figure 3.3 Typical pulse shapes in the time (left plots) and frequency (righ...

Figure 3.4 Example of pitting pulses recorded at the University of Bologna (...

Figure 3.5 Examples of PD pulse spectra from twisted pairs at different pres...

Figure 3.6 Different pulses waveform: (a) fast pulse with high-frequency con...

Figure 3.7 Energy probability density of electrons in air and SF_6 at 10 kV/m...

Figure 3.8 Slab of epoxy subjected to PD bombardment from a needle-plane ele...

Figure 3.9 Recognized stages of PD-induced degradation as time progresses to...

Figure 3.10 Tree propagation around a 5 mm-thick mica-barrier.

Figure 3.11 Tree channel formed at 20 °C and 15 kV in a polymer blend sample...

Figure 3.12 HV corona and LV corona.

Figure 3.13 Electric field lines in a point/plane electrode configuration an...

Figure 3.14 PD pattern from (left) HV and (right) LV corona. HV corona is me...

Figure 3.15 Typical waveform of Trichel pulses at p = 30 kPa in (a) pure Ar ...

Figure 3.16 Current waveforms of (a) Trichel pulse at V = 780 V and (b) puls...

Figure 3.17 Electrical tree starting from a cavity.

Figure 3.18 The solid curve represents the PD inception field as a function ...

Figure 3.19 In gray, region where a starting electron must be created by the...

Figure 3.20 Mean time between electrons as a function of the radius (spheric...

Figure 3.21 Simplified model to calculate the charge q displaced by a stream...

Figure 3.22 PD charge in a spherical cavity as the function of the field ins...

Figure 3.23 Modeling of the time behavior of the field inside a cavity and t...

Figure 3.24 Modeling of the behavior of internal field (E_i: continuous line)...

Figure 3.25 Photographs of the light emitted by PDs in nitrogen (with epoxy ...

Figure 3.26 PD events above PDIV.

Figure 3.27 Modeling behavior of the field inside a cavity and PD magnitudes...

Figure 3.28 Schematic representation of PD phenomena from a single cylindric...

Figure 3.29 Example of corona PD from needle connected to the high voltage: ...

Figure 3.30 Definition of inception phase angle and phase angle range for po...

Figure 3.31 PD patterns at different overvoltages for corona PD (needle conn...

Figure 3.32 PD patterns at different overvoltages for internal PD. Indirect ...

Figure 3.33 PD patterns at different overvoltages for surface PD (crack in e...

Figure 3.34 PD magnitude for corona, internal, and surface discharges. Posit...

Figure 3.35 PD repetition rate for corona, internal, and surface discharges....

Figure 3.36 PD Inception phase angle for corona, internal, and surface disch...

Figure 3.37 PD phase angle range for corona, internal, and surface discharge...

Figure 3.38 PD magnitude for three different types of surface discharges. Po...

Figure 3.39 PD repetition rate for three different types of surface discharg...

Figure 3.40 PD Inception phase for three different types of surface discharg...

Figure 3.41 PD phase range for three different types of surface discharges. ...

Figure 3.42 Example of packets in the PRPD pattern: (left) treeing in an epo...

Chapter 4

Figure 4.1 Photograph of a ceramic post insulator supporting the HV aluminum...

Chapter 5

Figure 5.1 Optical spectrum measured by a spectrometer of surface PD occurri...

Figure 5.2 Photograph of an OFIL Scaler UV camera (lower right corner) detec...

Figure 5.3 Acoustic response of surface PD vs frequency (the fainter line is...

Figure 5.4 Spectrum from a “gap discharge” of about 5–10 nC in air.

Figure 5.5 Spectrum from a gap discharge in SF_6 at 100 kPa under similar con...

Figure 5.6 Use of acoustic imaging camera being used on an energized 13.8 kV...

Figure 5.7 Surface PD at the stator slot exit from a motor stator winding en...

Figure 5.8 Corona detected from a post-insulator in a substation using an ac...

Figure 5.9 Acoustic image from a point-plane corona source (described in IEE...

Figure 5.10 Acoustic spectra from different types of discharging sources wit...

Chapter 6

Figure 6.1 Direct measurement circuit.

Figure 6.2 Indirect measurement circuit.

Figure 6.3 High-pass characteristic of a combined C_k–R_M sensor considering a...

Figure 6.4 The PD source is represented as (a) an ideal voltage source, (b) ...

Figure 6.5 Quadripole structure.

Figure 6.6 Closed and split core HFCTs.

Figure 6.7 Transfer function of a commercial HFCT used for PD detection.

Figure 6.8 Terminal of a 220 kV XLPE cable with a Rogowski coil (the blue lo...

Figure 6.9 The ABC model for the equipment under test where C_C is the capaci...

Figure 6.10 The equivalent circuit representing the ABC model. The capacitiv...

Figure 6.11 Divider ratio for the coupling capacitor.

Figure 6.12 Currents within the EUT.

Figure 6.13 Induced charge as a function of d/D.Note that the symbols us...

Figure 6.14 Time and frequency domain representation of two pulses with diff...

Figure 6.15 Principle of quasi-integration. The output of the filter is prop...

Figure 6.16 Response (in V) of a wide-band PD detector to a train of PD puls...

Figure 6.17 Response (in V) of a narrowband PD detector to a train of PD pul...

Figure 6.18 Calibration for the direct (top) and indirect (bottom) measuring...

Figure 6.19 Detection stage. A PD pulse is processed in the same way as the ...

Figure 6.20 A PD pulse injected at some point of a transmission line splits ...

Figure 6.21 Electric pulses, V(n003)-black and detector output V(n002)-green...

Figure 6.22 Output of the quasi-integration filter at the near end as a func...

Figure 6.23 Propagation of a pulse in a cable 180 m long. The cable is open ...

Figure 6.24 Measured attenuation in XLPE cables.

Figure 6.25 Attenuation of PD pulse spectral components as a function of dis...

Figure 6.26 Power cable equivalent circuit.

Figure 6.27 Simulation of a detector output as a function of distance betwee...

Figure 6.28 Optimum detection bandwidth. Cable attenuation data reported in ...

Figure 6.29 Impedance vs frequency for a 13.2 kV, 7000 HP, 1200 rpm motor st...

Figure 6.30 Two-port schematization of the EUT.

Figure 6.31 Calibrator structure.

Figure 6.32 Ideal calibrator pulse.

Chapter 7

Figure 7.1 Measured spectrum from PD in GIS, measured with a UHF sensor.

Figure 7.2 Spectrum of EM fields irradiated from PD in air from a pair of ma...

Figure 7.3 Due to the reciprocal cancellation of positive and negative half ...

Figure 7.4 PD spectra measured within a metallic tank equipped with a medium...

Figure 7.5 EM far- and near-field patterns.

Figure 7.6 Fraunhofer distance as a function of EM wave frequency and emitti...

Figure 7.7 Frequency-dependent EM wave intensity in a three-phase gas-insula...

Figure 7.8 Attenuation of an RG-213 U coaxial cable.

Figure 7.9 Connection link structures.

Figure 7.10 Example of readings from a four-channel oscilloscope connected t...

Figure 7.11 The Prysmian Prycam detector is an example of peak detector oper...

Figure 7.12 Partial discharges in a power transformer detected using an UHF ...

Figure 7.13 Example of PD pattern reconstructed using a (time-domain) oscill...

Figure 7.14 Magnetic loop operation principle.

Figure 7.15 Doble TEV sensor (left) picture of the sensor.(right) operat...

Figure 7.16 Techimp-Altanova TEV sensor (left) picture of the sensor.(ri...

Figure 7.17 GIS electric field sensors: diagram (left) and example (right)....

Figure 7.18 A transformer drain valve with combined UHF and acoustic sen...

Figure 7.19 (left) GIS UHF flange sensor.UHF PD dielectric window plate ...

Figure 7.20 Patch antenna: (left) photograph of a 2.4 GHz patch antenna....

Figure 7.21 Horn antenna structure.

Figure 7.22 Simplified schematics of SSC.

Figure 7.23 Principle of sensitivity check: (top) detection at C2 during ope...

Figure 7.24 Comparison of the spectra in the UHF range for a 5 pC pulse and ...

Chapter 8

Figure 8.1 Block diagram of a mixed analog and digital detector.

Figure 8.2 Block diagram of a typical all-digital PD detector where the orig...

Figure 8.3 All digital detector where the waveform of each pulse is stored, ...

Figure 8.4 Block diagram of a UHF PD sensor that can be connected to an LF o...

Figure 8.5 Schematic of two sensors per phase using the time-of-flight metho...

Figure 8.6 Example of VHF PRPD plots collected online from Phase A of a gene...

Figure 8.7 Photo of an 80 pF PD detection capacitor intended for permanent i...

Figure 8.8 PMA plot of PD from a stator coil measured in the VHF range.

Figure 8.9 *Ø-q-n* chart of the same data shown in Figure 8.8...

Figure 8.10 PRPD chart of the same data shown in Figure 8.9.

Figure 8.11 Higher resolution PRPD plot using an LF (IEC 60270-compatable) d...

Figure 8.12 PD trend plot of the peak positive PD magnitude collected at the...

Figure 8.13 Typical PDIV/PDEV chart using a LF PD detector on a stator coil....

Figure 8.14 Plot of PD magnitude Q_m vs generator load for a 13.8 kV, 225 MVA...

Figure 8.15 Example of application of the *TF* map on an air-cooled turbogener...

Figure 8.16 Example of the recording of a single event on Phase L2 (left plo...

Figure 8.17 Three-dimensional amplitude comparison chart (upper left) for a ...

Figure 8.18 PRPD plots from an online VHF measuring system. The vertical sca...

Chapter 9

Figure 9.1 PRPD plot of noise across the AC cycle caused by electronic switc...

Figure 9.2 Oscilloscope image of static exciter pulses superimposed on the r...

Figure 9.3 Example of an analog balanced bridge to suppress interference fro...

Chapter 10

Figure 10.1 Interphasal PD (white powder) occurring on a stator winding betw...

Figure 10.2 Photo of PD between the phase buses in a 13.8 kV metalclad air-i...

Figure 10.3 Trend in PD magnitude in a power cable where the joint failed af...

Figure 10.4 Trend in $+Q_m$ (blue) and $-Q_m$ (orange) measured online over an 18-...

Figure 10.5 Cross-section of a stator coil in slot with PD occurring at thre...

Figure 10.6 PRPD plot from a lab test on a 4.1 kV motor coil. The vertical s...

Figure 10.7 Sketch of the positive and negative PRPD pattern outlines as pro...

Figure 10.8 Idealized PRPD patterns from various types of defects in an insu...

Figure 10.9 Rabbit ear PRPD pattern.

Figure 10.10 Vector diagram showing the relationship between the phase to ne...

Figure 10.11 PD patterns for interphasal PD between A and B phases, when dis...

Figure 10.12 Equivalent circuit of a single PD pulse occurring in the air ga...

Figure 10.13 Sketches of PRPD plots where PD is occurring in Phase A, that i...

Figure 10.14 (c) on the next page, shows the idealized PRPD pattern when two...

Chapter 11

Figure 11.1 PD polarity analysis for direct and indirect circuits. *Ck* is the...

Figure 11.2 Direct and indirect detection circuit for instrument voltage tra...

Figure 11.3 Direct and indirect detection circuit for instrument current tra...

Figure 11.4 Sensitivity check procedure.

Chapter 12

Figure 12.1 Structure of power cable (left) without semiconductive layers; (...

Figure 12.2 Cross section of an old submarine 30 kV mass-impregnated cable. ...

Figure 12.3 Cross section of 400 kV polymeric cable.

Figure 12.4 Electric field and equipotential lines in a coaxial cable with i...

Figure 12.5 Stress cone (black, partly conductive material) embedded in a me...

Figure 12.6 Effect of nonlinear stress control tubes in a coaxial cable with...

Figure 12.7 Comparison between terminations: (left) cable to air-insulated s...

Figure 12.8 Power cable manufacturing defects leading to PD activity.

Figure 12.9 Example of water tree.

Figure 12.10 Propagation of PD activity in a taped insulation.

Figure 12.11 High-voltage cable joint for extruded cables.

Figure 12.12 Wet-type terminations of MI cables with draining mass.

Figure 12.13 High-voltage cable termination with a HFCT and a Rogowski coil ...

Figure 12.14 Connections of the shields in the link box (a) in operation, (b...

Figure 12.15 Link box prepared for PD measurement with a HFCT on a jumper ca...

Figure 12.16 Principle of operation of joint capacitive couplers.

Figure 12.17 HFCTs clamped around the coaxial cables for shield transition....

Figure 12.18 Simulation of the electric field created by the partial dischar...

Figure 12.19 Spherical antenna (differential field probe) sensors.

Figure 12.20 Flexible magnetic coupler (FMC): (left) sketch of the structure...

Figure 12.21 PD pulse peak voltage as a function of distance propagated (cal...

Figure 12.22 Optimum detection bandwidth as a function of the distance betwe...

Figure 12.23 Example of structure of temporary HV water termination for PD t...

Figure 12.24 450 kV, 700 MVAR subsea cable testing resonant test set that in...

Figure 12.25 Scheme of a variable AC frequency RTS.

Figure 12.26 Schematic of an OWTS.

Figure 12.27 Effect of PD activity in one defective joint after only one hou...

Figure 12.28 Permanent power supply (PPS) that can be used to power instrume...

Figure 12.29 Cable system used for the demonstration of PD monitoring effect...

Figure 12.30 TF map analysis of the phenomena recorded in the cable system r...

Figure 12.31 Monitoring of phenomenon A in the cable system of Figure 12.29,...

Figure 12.32 Monitoring of phenomenon B in the cable system of Figure 12.29,...

Figure 12.33 Noise in a 223 m-long cable laid above the ground.

Figure 12.34 Propagation of a calibrator pulse through a 20 km-long cable....

Figure 12.35 Derivation of the 3PTRD diagram. Left: Visualization segments o...

Figure 12.36 Example of PD measurement analysis in a healthy joint of a cabl...

Figure 12.37 Example of PD measurement analysis in a faulty joint of a cable...

Figure 12.38 Examples of PRPD pattern due to PD internal to cable systems an...

Figure 12.39 Example of TDR measurements on a digital oscilloscope (Rebound ...

Figure 12.40 Example of TDR-based PD location mapping.

Figure 12.41 Example of ToA location localization.

Figure 12.42 Example of readings from a ToA localization used in the cable s...

Figure 12.43 Sketch of GPS-synchronized ATA localization system.

Figure 12.44 Estimated behavior of PD pulse peak value, equivalent time, *T*, ...

Figure 12.45 AF mapping of discharges on an outdoor insulator located at ter...

Figure 12.46 AF mapping of discharges within a section of a cable. The ampli...

Chapter 13

Figure 13.1 Some examples of GIS. (with permission: Hitachi Energy (left), S...

Figure 13.2 Typical components of GIS.

Figure 13.3 Examples of epoxy insulating spacers in GIS; one for three-phase...

Figure 13.4 Photo showing insulating paint on GIS enclosure.

Figure 13.5 Proportion of failures in GIS/GIL due to dielectric defects (blu...

Figure 13.6 Simplified diagram showing typical PD defects in GIS.

Figure 13.7 Photos showing some examples of particles found in GIS.

Figure 13.8 Conceptual diagram of a floating potential discharge.

Figure 13.9 Conceptual diagram of a protrusion in GIS as a “needle-plane” ge...

Figure 13.10 Photo showing damage following cable-end termination failures....

Figure 13.11 Photo showing surface tracking caused by a particle lying on th...

Edition

Paul Krause, Oleg Wasynczuk, Steven D. Pekarek, and Timothy O'Connell

97. *Applications of Modern Heuristic Optimization Methods in Power and Energy Systems*

    Kwang Y. Lee and Zita A. Vale

98. *Handbook of Large Hydro Generators: Operation and Maintenance*

    Glenn Mottershead, Stefano Bomben, Isidor Kerszenbaum, and Geoff Klempner

99. *Advances in Electric Power and Energy: Static State Estimation*

    Mohamed E. El-hawary

100. *Arc Flash Hazard Analysis and Mitigation, Second Edition*

    J.C. Das

101. *Maintaining Mission Critical Systems in a 24/7 Environment, Third Edition*

    Peter M. Curtis

102. *Real-Time Electromagnetic Transient Simulation of AC-DC Networks*

    Venkata Dinavahi and Ning Lin

103. *Probabilistic Power System Expansion Planning with Renewable Energy Resources and Energy Storage Systems*

    Jaeseok Choi and Kwang Y. Lee

104. *Power Magnetic Devices: A Multi-Objective Design Approach, Second Edition*

Scott D. Sudhoff

105. *Optimal Coordination of Power Protective Devices with Illustrative Examples*

Ali R. Al-Roomi

106. *Resilient Control Architectures and Power Systems*

Craig Rieger, Ronald Boring, Brian Johnson, and Timothy McJunkin

107. *Alternative Liquid Dielectrics for High Voltage Transformer Insulation Systems: Performance Analysis and Applications*

Edited by U. Mohan Rao, I. Fofana, and R. Sarathi

108. *Introduction to the Analysis of Electromechanical Systems*

Paul C. Krause, Oleg Wasynczuk, and Timothy O'Connell

109. *Power Flow Control Solutions for a Modern Grid using SMART Power Flow Controllers*

Kalyan K. Sen and Mey Ling Sen

110. *Power System Protection: Fundamentals and Applications*

John Ciufo and Aaron Cooperberg

111. *Soft-Switching Technology for Three-phase Power Electronics Converters*

Dehong Xu, Rui Li, Ning He, Jinyi Deng, and Yuying Wu

112. *Power System Protection, Second Edition*

Paul M. Anderson, Charles Henville, Rasheek Rifaat, Brian Johnson, and Sakis Meliopoulos

113. *High Voltage and Electrical Insulation Engineering, Second Edition*

Ravindra Arora and Wolfgang Mosch.

114. *Modeling and Control of Modern Electrical Energy Systems*

Masoud Karimi-Ghartemani

115. *Control of Power Electronic Converters with Microgrid Applications*

Armdam Ghosh and Firuz Zare

116. *Coordinated Operation and Planning of Modern Heat and Electricity Incorporated Networks*

Mohammadreza Daneshvar, Behnam Mohammadi-Ivatloo, and Kazem Zare

117. *Smart Energy for Transportation and Health in a Smart City*

Chun Sing Lai, Loi Lei Lai, and Qi Hong Lai

118. *Wireless Power Transfer: Principles and Applications*

Zhen Zhang and Hongliang Pang

119. *Intelligent Data Mining and Analysis in Power and Energy Systems: Models and Applications for Smarter Efficient Power Systems*

Zita Vale, Tiago Pinto, Michael Negnevitsky, and Ganesh Kumar Venayagamoorthy

120. *Introduction to Modern Analysis of Electric Machines and Drives*

Paul C. Krause and Thomas C. Krause

121. *Electromagnetic Analysis and Condition Monitoring of Synchronous Generators*

Hossein Ehya and Jawad Faiz

122. *Transportation Electrification: Breakthroughs in Electrified Vehicles, Aircraft, Rolling Stock, and Watercraft*

    Ahmed A. Mohamed, Ahmad Arshan Khan, Ahmed T. Elsayed, Mohamed A. Elshaer

123. *Modular Multilevel Converters: Control, Fault Detection, and Protection*

    Fuji Deng, Chengkai Liu, and Zhe Chen

124. *Stability-Constrained Optimization for Modern Power System Operation and Planning*

    Yan Xu, Yuan Chi, and Heling Yuan

125. *Interval Methods for Uncertain Power System Analysis*

    Alfredo Vaccaro

126. *Practical Partial Discharge Measurement on Electrical Equipment*

    Greg C. Stone, Andrea Cavallini, Glenn Behrmann, and Claudio Angelo Serafino